Rheology and Morphology of Smectic Liquid Crystal/Polymer Blends

Jun Yonezawa,† Stephen M. Martin, Christopher W. Macosko,* and Michael D. Ward

Department of Chemical Engineering and Materials Science, University of Minnesota, 421 Washington Avenue SE, Minneapolis, Minnesota 55455

Received March 30, 2004; Revised Manuscript Received June 10, 2004

ABSTRACT: Polymers are often blended with additives (e.g., polymers, clays) to produce composite materials having desirable physical properties that reflect synergy between the blend constituents. Though polymer blends with small-molecule nematic liquid crystal phases have been investigated (primarily for displays), related materials containing small-molecule smectic phases have not been reported. Guanidinium alkylbenzenesulfonates (GC*n*BS, where *n* is the number of carbons in the alkyl chain), which form stable smectic phases at elevated temperatures because of a robust two-dimensional hydrogen-bonding network of guanidinium ions and sulfonate moieties, were melt-blended with various polymers. Rheological characterization of the blends reveals a yielding behavior, characteristic of the pure GC*n*BS smectic phases, which becomes more pronounced with increasing GC*n*BS concentration. Two microstructures—one a continuous polymer phase embedded with GC*n*BS droplets and the other a continuous GC*n*BS phase with a discontinuous polymer phase—are observed, the latter at GC*n*BS concentrations as low as 2 wt %. The tendency of the blends to form a microstructure in which GC*n*BS is continuous requires the existence of a smectic phase (observed only for $n \geq 7$) and is dependent on alkyl chain length and GC*n*BS concentration. Injection of molten blends containing smectic phases into a rectangular mold resulted in stratification of the rectangular composite plaque due to the formation of large two-dimensional crystalline lamellae upon cooling of the GC*n*BS smectic phase dispersed in the blend. This stratification, which can be attributed to large extensional stresses experienced by the blend during molding, depends on alkyl chain length, GC*n*BS concentration, and the magnitude of the stresses exerted on the molten blend. These results illustrate that smectic phases can promote unusual microstructures in polymer blends at very low concentrations, which may be useful in certain commercial applications.

Introduction

Polymer-based composites and blends have received considerable attention owing to the prospect of achieving materials with properties and functions that cannot be realized with the individual components alone. The multicomponent nature of these materials often provides additional degrees of freedom with respect to the control and manipulation of properties and functions, particularly when the components are characterized by different length scales tailored to introduce synergistic functionality. For example, low molecular weight liquid crystals, typically nematic, have been combined with polymers for applications in electrooptic displays and membranes,[1−7] wherein the polymer provides confinement and mechanical reinforcement for the functional liquid crystal component. The phase behavior of high molecular weight liquid crystal polymers has been exploited in polymer blends to facilitate processing.[8−10]

Polymer composites made with clays, such as montmorillonite, have exhibited increased modulus, reduced gas permeability and reduced thermal expansion, effects that rely on ultrathin clay platelets, present in relatively small amounts, dispersed throughout the polymer. Reduction in gas permeability is associated with tortuosity introduced by the highly dispersed clay platelets, which often are aligned parallel to the membrane through shear.[11] Improved modulus and reduced thermal expansion in such materials stems from high stiffness of the clay and the substantial interfacial contact area between the clay platelets and the polymer.[12,13]

The mechanical properties of polymers can also be manipulated by the introduction of constituents with hydrogen-bonding groups. For example, "supramolecular polymers" display unique rheological properties due to the reversibility of the hydrogen-bonding interactions between mesogenic or polymeric components.[14] Small molecule additives with hydrogen bonding groups, such as 1,3:2,4-dibenzylidenesorbitol or various substituted binary complexes of barbiturates and 2,4,6-triaminopyrimidines, spontaneously form three-dimensional continuous fibrillar networks in host polymers.[15−18] These networks, in both the melt and crystalline state, can produce measurable effects on the mechanical properties of the blends at low concentrations of the small molecule component (<3%).

Blend and composite microstructures and their associated mechanical properties are central to the applications of these materials. The microstructures can be characterized by their dimensionality, which range from droplets (0-D) to fibers (1-D) to lamellae (2-D) to co-continuous phases (3-D). The lamellar microstructure, which is of particular interest for a number of technologies (e.g., barrier films, birefringent coatings), can be produced by specialized processing methods.[19] Direct formation of lamellar microstructures by spontaneous phase separation, however, often is more desirable as it allows for more facile processing.[20] One possible strategy for achieving spontaneous formation of lamellar microstructures involves the self-assembly of small molecules into 2-D hydrogen-bonded networks

† Asahi Kasei Corporation, 1-3-1, Yakoh, Kawasaki-ku, Kawasaki-city, Kanagawa 210-0863, Japan.

* To whom correspondence should be addressed. E-mail: macosko@umn.edu.

10.1021/ma0493729 CCC: $27.50
Published on Web 07/30/2004

that promote stratification during blend processing. If these networks are able to form crystalline phases (i.e., upon cooling of a blend), they may naturally form nanometer-scale crystalline platelets dispersed throughout the host polymer, providing an alternative to the aforementioned polymer clay composite. To our knowledge, polymer blends that incorporate small molecule components capable of forming 2-D networks that promote lamellar microstructures have not been reported.

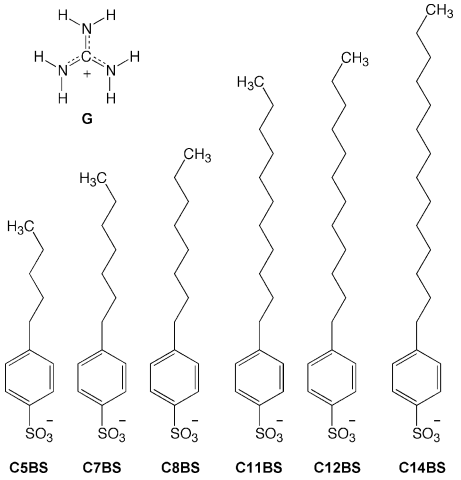

One of our laboratories has reported numerous crystalline organic materials, with a variety of layered architectures, based on a highly persistent 2-D hydrogen-bonded network of topologically complementary guanidinium (**G**) ions, $C(NH_2)_3^+$, and sulfonate moieties (**S**) of organomonosulfonate and organodisulfonates.[21−24] The **GS** sheets, which typically adopt a "quasihexagonal" motif, are separated by the organic residues of the organosulfonates. Recently, certain guanidinium alkylbenzenesulfonates (GC*n*BS where *n* refers to the number of carbons in the alkyl chain) were reported to form *smectic* liquid crystalline phases at elevated temperatures.[25] Although the structures of the crystalline phases (i.e., room temperature) and the corresponding smectic phases were only surmised by extrapolation from the previously reported single-crystal structure of GC1BS,[26] the *d*-spacings for the smectic phases were consistent with the existence of a bilayer-like architecture, similar to that observed for many crystalline **GS** compounds. Our laboratory since has determined that several of the crystalline GC*n*BS phases, however, do not exhibit a simple bilayer structure.[27] The absence of any nematic phases for these compounds illustrates that the hydrogen-bonded **GS** network enforces the smectic architecture.

The layered architectures of crystalline GC*n*BS compounds are reminiscent of the aforementioned clays, which have been used to prepare polymer-based composites with superior elastic modulus and gas barrier properties. The GC*n*BS compounds, however, self-assemble to form crystalline phases at ambient temperature and smectic phases at temperatures typically used for processing polymers. Furthermore, the organic moieties in this class of materials, which are covalently anchored to the 2-D hydrogen-bonded network, can be adjusted systematically to tailor the compatibility of the **GS** compounds with various polymers. (The dispersal of clays in host polymers typically relies on the adsorption of ionic surfactants to the charged surfaces of the clays as well as the application of high shear stresses.) This suggests an opportunity to produce composite materials in which the smectic phases, present as a minor component, form ultrathin crystalline platelets dispersed throughout the polymer matrix or large-scale layered structures spanning the cross section of a polymer plaque. Notably, polymers coated with ultrathin films of hydrogen-bonded networks were reported to exhibit improved gas barrier properties, illustrating the technological promise of composites containing 2-D molecular networks.[28] The unique features of the GC*n*BS compounds prompted us to examine the microstructure and rheology of blends based on small amounts of these compounds and homopolymers. Herein we describe our initial investigations of these blends, which reveal the tendency of the hydrogen-bonded smectic phases to form dispersed 2-D networks that promote stratification of the polymer, particularly when the polymer/GC*n*BS(smectic) blend experiences high stresses during melt processing.

Table 1. Isotropic Melting Temperatures ($T_{C\rightarrow I}$) and Smectic Transition Temperatures ($T_{C\rightarrow S}$) for Selected GC*n*BS Compounds

	$T_{C\rightarrow I}$ (°C)	$T_{C\rightarrow S}$ (°C)
GC5BS	201.7	
GC7BS		174.7
GC8BS		180.3
GC11BS		140.7
GC12BS		130.9
GC14BS		122.7

Results and Discussion

Polymer/GC*n*BS Blends. It is reasonable to expect that the hydrogen bond enforcement of the smectic GC*n*BS phases would be preserved during high-temperature processing of blends based on homopolymers and small amounts of these compounds, leading to the formation of 2-D hydrogen-bonded networks throughout the homopolymer. The resulting blends would be expected to exhibit microstructures and rheological signatures that differ substantially from those observed for the aforementioned fibrillar hydrogen-bonded networks. Conveniently, both the ability of the GC*n*BS compounds to form smectic phases and the smectic transition temperatures ($T_{C\rightarrow S}$) depend on alkane chain length (Table 1). Compounds with $n < 7$ exhibit only isotropic melting points ($T_{C\rightarrow I}$); the melts decompose at elevated temperatures ($T > 250$ °C) with no smectic phase observed. Smectic phases are observed for $n \geq 7$, the $T_{C\rightarrow S}$ values decreasing with increasing chain length. The dependence of $T_{C\rightarrow S}$ on chain length allows one to choose smectic phases that are compatible with desired processing conditions and polymer properties (e.g., T_m, T_g). The processing temperature employed herein for polymer melt blending and injection molding exceeds the highest $T_{C\rightarrow I}$ and $T_{C\rightarrow S}$ temperatures for the GC*n*BS compounds, thereby ensuring formation of the isotropic melt or smectic phases under these conditions. Furthermore, the $T_{C\rightarrow I}$ and $T_{C\rightarrow S}$ for the GC*n*BS compounds in Table 1 ensures formation of crystalline phases in all cases upon cooling to room temperature.

Polymer/GC*n*BS melt blending was performed by mixing, under a nitrogen atmosphere, a homopolymer (polystyrene, polypropylene, or high-density polyethylene) and GC*n*BS at a temperature above $T_{C\rightarrow S}$ of the small molecule and T_m or T_g of the polymer (Figure 2) followed by extrusion through a cylindrical die to

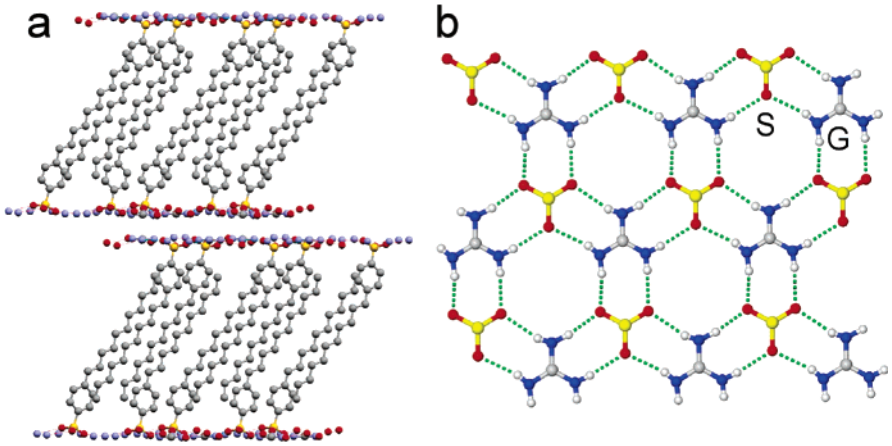

Figure 1. (a) Side view of the crystal structure of GC11BS, which adopts a layered packing arrangement in which layers of alkylbenzene moieties are separated by hydrogen-bonded **GS** sheets. (b) Top view of the 2-D "quasi-hexagonal" network formed by complementary hydrogen-bonding between guanidinium (**G**) ions and the sulfonate (**S**) moieties of organosulfonates. (The organic residues of the organosulfonates are omitted for clarity.)

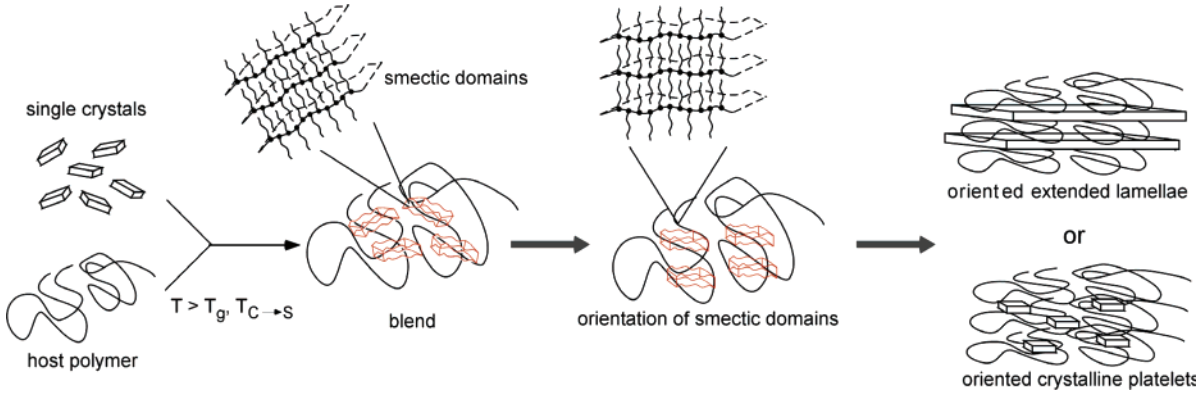

Figure 2. Schematic representation of melt processing of polymer/smectic GC*n*BS blends.

generate 2 mm diameter cylindrical strands. Injection molding was performed by remelting these strands at the same processing temperature and injecting the melt into a rectangular mold held at a temperature of 70 °C. Two molds of different thickness (1 and 2 mm) were used to compare the effect of varying the stresses applied during molding on the final composite microstructure.

Polarized optical microscopy and powder X-ray diffraction (PXRD) confirmed the existence of the smectic phases in molten polypropylene and PS/GC*n*BS blends, as illustrated in Figure 3 for PP/5% GC11BS and PS/5% GC14BS, respectively. The optical micrographs reveal the maltese cross pattern typical of spherulitic lamellae. The PXRD reveals a narrow peak at a low 2θ value, assignable to the layer spacing of the smectic phase (confirmed by comparison with the pure material) and diffuse scattering associated with PS. Upon cooling to room temperature, the PXRD of the blends was consistent with the formation of crystalline GC*n*BS, displaying pronounced (002) and (004) reflections. The (002) reflection appears at a slightly higher 2θ value than the peak associated with the smectic phase, indicating a slightly expanded layer spacing in the smectic than in its crystalline counterpart.

The rheological behavior of pure GC*n*BS smectic phases is reported in detail elsewhere,[27] but a brief description here is useful for understanding the properties of polymer blends containing these components. These rheology measurements were performed under steady shear, wherein the viscosity was measured as samples were sheared at a constant rate between two parallel plates. Immediately following the application of shear at 220 °C ($> T_{C\rightarrow S}$) the viscosities of the pure GC*n*BS smectic phases increased gradually to ca. 10^3 Pa·s, as illustrated in Figure 4 for GC12BS, followed by noticeable yielding at a strain value of approximately 1. The observation of a yield point is regarded as diagnostic of shear-induced alignment of lamellar smectic domains.[27] The viscosities beyond this yield point approached a constant value of approximately 3×10^2 Pa·s. The viscosities of the GC*n*BS liquid crystals are essentially independent of the alkylbenzenesulfonate chain length, including the ones employed here ($n = 8$, 11, 12, and 14), except for GC7BS, which exhibits lower viscosity values across the entire range of strain values. Overall, the viscosities of the GC*n*BS smectic phases were substantially larger than values reported for other smectic phases (e.g., diethyl-4,4′-azoxydibenzoate, cholesteryloleate, 4-octyl-4′-cyanobiphenyl) or nematic liquid crystals such as the nematic phase of 4-octyl-4′-cyanobiphenyl.[29] This can be attributed to the structural reinforcement provided by the hydrogen-bonded **GS** network and argues that the smectic architecture is retained during shear, including blend processing.

Unlike the pure smectic phases, the steady shear viscosity of pure PS, as expected, did not exhibit yielding behavior. The blends, however, do exhibit yield that is very sensitive to the concentration of the smectic component, as illustrated in Figure 4a for PS/GC12BS (5 and 10 wt % GC12BS). Pure GC*n*BS and the PS/GC*n*BS blends also exhibit shear thinning (Figure 4b),

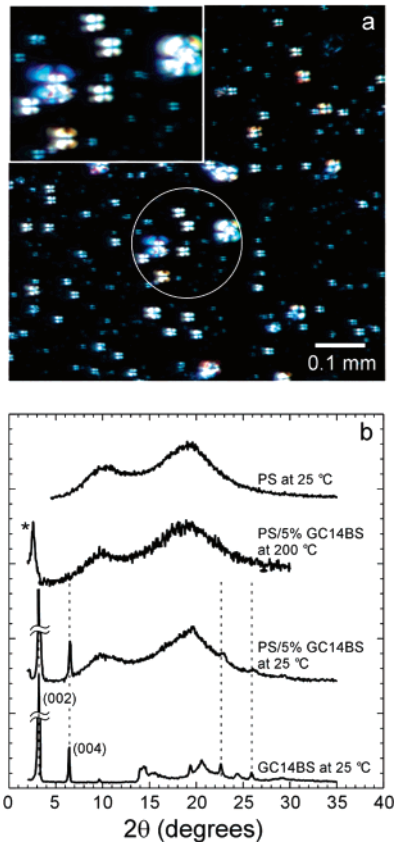

Figure 3. (a) Optical micrograph of a polypropylene/5% GC11BS blend acquired at 180 °C using polarized light, revealing the maltese cross pattern that is diagnostic of the spherulites of the smectic phase. (b) Powder XRD patterns for bulk crystalline GC14BS after cooling from the smectic phase, PS, injection-molded PS/5% GC14BS, all at room temperature, and molten PS/5% GC14BS at 200 °C. The two lowest peaks (in 2θ), which correspond to the (002) and (004) reflections (d_{002} = 28.505 Å; d_{004} = 14.03 Å), are observed in both bulk GC14BS and the blend at room temperature. The molten blend exhibits a sharp peak (∗) at low 2θ (d = 35.13 Å), which is characteristic of the smectic phase.[14]

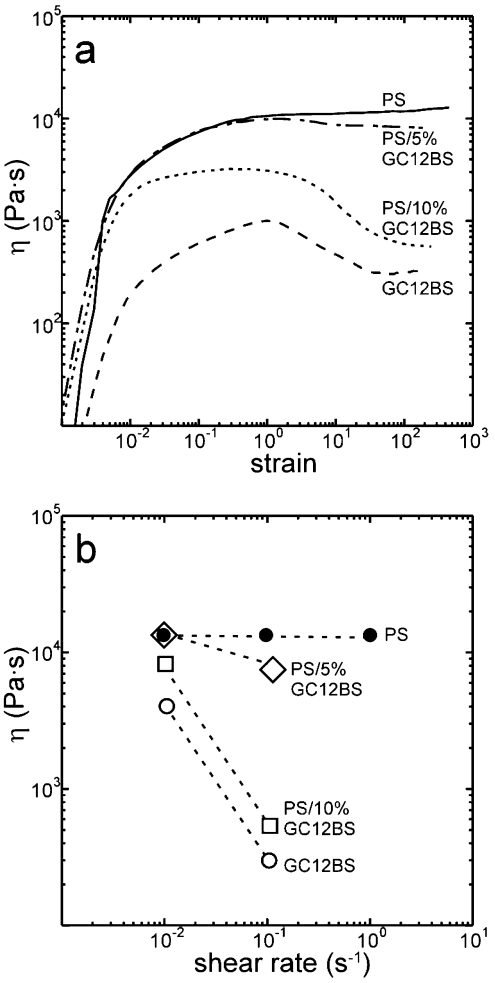

Figure 4. (a) Viscosities measured under steady shear for PS, PS/5% GC12BS, PS/10% GC12BS, and pure GC12BS at 220 °C and a shear rate of 0.1 s^{-1}. (b) The constant viscosity measured beyond the yield point for pure PS, PS/5% GC12BS (open diamonds), PS/10% GC12BS (open squares), and pure GC12BS (open circles) at a temperature of 220 °C. As expected, pure PS does not exhibit shear thinning.

similar to behavior reported for other smectic liquid crystals.[30]

Microstructure of Extruded PS/GC*n*BS Blends. Extruded cylindrical strands of the PS/GC*n*BS blends exhibited two distinct microstructures: one in which the PS phase is continuous and surrounds discontinuous GC*n*BS "droplets" and one in which the GC*n*BS smectic phase is continuous and surrounds discontinuous PS particles. These microstructures were evident from scanning electron microscopy (SEM) of strands that had been "developed" by soaking the blends with methanol at room temperature to dissolve and remove the GC*n*BS component that crystallized from the isotropic melt or smectic phases upon cooling to room temperature. The microstructure characterized by SEM, therefore, was a replica of the microstructure existing in the molten blend under shear. For example, a PS/15% GC5BS blend revealed hollow features that resulted from the removal of spherulitic crystals embedded in the PS matrix, signifying the presence of GC5BS droplets in the molten state (Figure 5a). Blends of PS with GC5BS, which forms an isotropic melt, produced the droplet microstructure at all concentrations examined (1−15 wt %).

Blends containing certain concentrations of GCnBS smectic ($n \geq 7$) components exhibited a markedly different microstructure (Figure 5b). These blends disintegrated upon soaking in methanol to produce particles and fibers of PS bearing imprints of GC*n*BS crystallites on their surfaces (Figure 6). This is indicative of the blend microstructure that is continuous in the minor smectic component and in which large droplets of PS are sequestered by the smectic phase. The observation of a discontinuous polymer phase is quite distinct from the microstructures observed in the aforementioned polymer blends, in which small molecule additives form networks of hydrogen-bonded fibrils that are incapable of sequestering the polymer component.[15−18] Furthermore, the concentrations required for achieving discontinuous phases in polymer−polymer blends[31] are substantially higher than those observed here for the smectic GC*n*BS compounds. The existence of a discontinuous PS phase in some of the PS/GC*n*BS blends is corroborated by their brittle character, in contrast with the blends having a droplet microstructure, which are ductile. The two microstructures also differ with respect to their optical transparency; the discontinuous PS microstructure is opaque whereas the droplet microstructure is translucent. Finally, the rheological characteristics of the corresponding melts of the two microstructures are significantly different; the droplet microstructure exhibits little yielding on shearing—behavior akin to the pure PS—while the

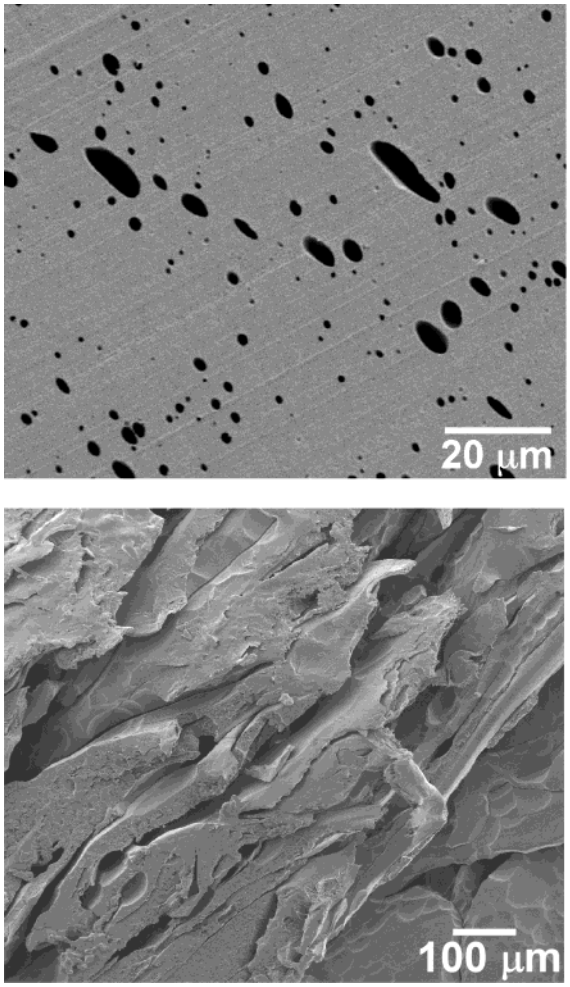

Figure 5. (a, top) SEM image of the microstructure of an extruded strand of a PS/15% GC5BS blend after microtoming and removal of GC5BS via dissolution in methanol, exhibiting the characteristic droplet microstructure of GC*n*BS within a PS matrix. (b, bottom) SEM image of the microstructure of a PS/15% GC14BS blend after fracture and prior to dissolution of the GC14BS phase.

discontinuous PS microstructure exhibits significant yielding upon shearing—behavior that is closer to that of the pure GC*n*BS smectic phases (Figure 4).

These results indicate that the smectic nature of the GC*n*BS component induces the formation of walls, where the nonpolar phenylalkane tails are in contact with the PS, that separate PS fibers and spheres. Continuity is maintained throughout the blend due to reinforcement by intermolecular guanidinium−sulfonate hydrogen bonding. The discontinuous character of the PS phase rules out a fibrillar-like GC*n*BS network based on one-dimensional "tapes". It may seem surprising that small quantities of a smectic liquid crystal phase, which is naturally 2-D in character, would form a continuous network in three dimensions. Calculations based on a rudimentary model that assume spherical PS particles, however, demonstrate that for a PS particle size of 200 μm (comparable to those observed here) a 2% GC8BS smectic network having a nominal wall thickness of approximately 1 μm is sufficient to support a continuous network.[32] Indeed, this model predicts that a continuous smectic network with a wall thickness corresponding to two bilayers (ca. 60 Å) can be achieved at 2 wt % even if the total PS surface area is increased by reducing the particle diameter to 170 nm.

The absence of a continuous GC5BS phase for any concentration (Figure 7), coupled with the observation of continuous GC*n*BS phase for $n \geq 7$ at certain concentrations, clearly indicates that *a smectic phase is required to achieve a continuous GCnBS component during melt processing*. Surprisingly, the weight fraction needed to form the continuous GC*n*BS phase increases with *n*; for example, continuous GC14BS was observed at 15 wt % but not at 10 wt %.

Upon extrusion of cylindrical strands of polymer blends with compositions in the droplet region (Figure 7), the GC*n*BS droplets are subjected to shear stresses imposed by the die, thereby producing elongated droplets that can be characterized by a cylinder length, *L*, and a cross-sectional diameter, *D*. These parameters can be measured directly by inspection of sample surfaces that have been exposed by microtoming the strands parallel and perpendicular to the extrusion direction, respectively (Figure 8). The average value of *D* for GC5BS, which forms an isotropic melt, depends more strongly on concentration than either GC12BS or GC14BS, which form smectic liquid crystal phases (Figure 9). This indicates that for a given concentration the GC*n*BS smectic phases support the existence of small, extended droplets better than the isotropic GC5BS melt, which apparently prefers to coalesce into larger droplets as the concentration is increased.[33] Furthermore, the average values of *L* and the *L*/*D* ratios for the GC12BS and GC14BS smectics are larger than those of PS/GC5BS, and the *L*/*D* value for GC12BS is roughly twice that observed for GC14BS. The larger values of *L*/*D* for the smectic phases, which are tantamount to a larger surface area-to-volume ratio, are likely due to the influence of the 2-D lamellar structure of the hydrogen-bond reinforced smectic, which makes the formation of extended structures more favorable. The larger *L*/*D* value for GC12BS with respect to GC14BS most likely reflects a lower interfacial energy between the smectic phase and the polymer for shorter alkyl chain lengths. The relationship between the interfacial energy and the drop morphology (i.e., the *L*/*D* ratio) can be understood in terms of theory that relates the stability of extended droplets to capillary number (*Ca*).[34] Extended droplets (i.e., large *L*/*D* ratio) are more stable when $Ca \gg 1$, a condition favored by small interfacial energy. A low interfacial energy, indicated by a high *Ca*, would be consistent with the tendency of the smectic component to form a continuous phase that requires substantial interfacial contact area between the polymeric and smectic components.

Microstructure of Injection-Molded PS/GC*n*BS Blends. The two-dimensional character of the crystalline GC*n*BS salts and their corresponding smectic phases suggests that large-area hydrogen-bonded lamellae of these salts, possibly spanning a rectangular polymer plaque, may be achievable under conditions that promote extensional flow in two dimensions. SEM revealed that the GC*n*BS domains in the extruded cylindrical strands reverted to spherical droplets upon annealing at 220 °C. Injection of these molten PS/GC5BS blends produced rectangular plaques with platelike domains of GC5BS throughout the molded plaque, in contrast with the extended droplets observed in the extruded cylindrical strands (Figure 10). Injection molding of *smectic* GC*n*BS blends in a 1 mm thick mold produced platelike GC*n*BS domains, similar to those observed for GC5BS blends, in the interior of the plaque,

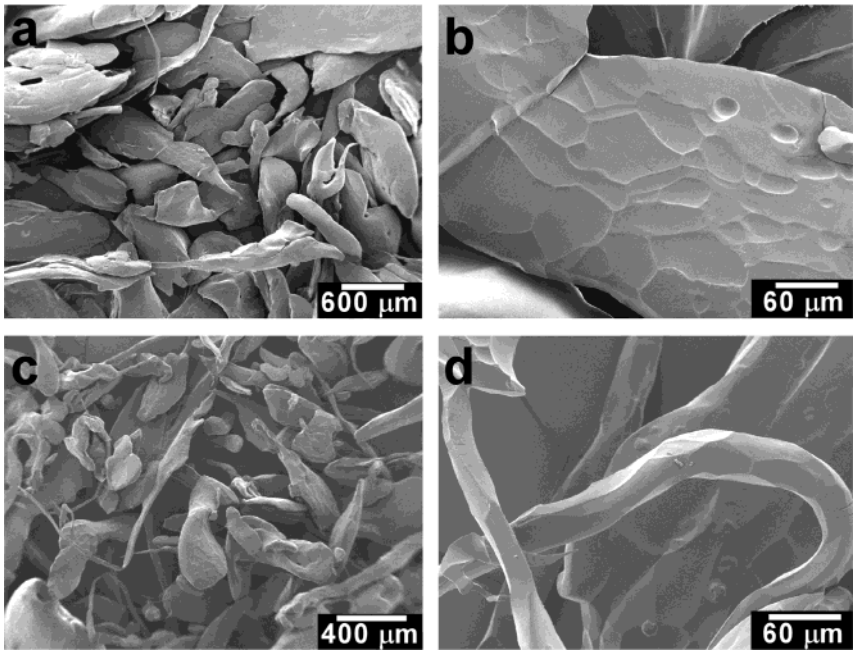

Figure 6. SEM images of extruded blends of (a, b) PS/2% GC8BS and (c, d) PS/5% GC11BS after the removal of GC*n*BS by dissolution in methanol. The breakup of the strands into small particles upon removal of GCnBS indicates that even at low concentrations a GC*n*BS continuous microstructure is formed.

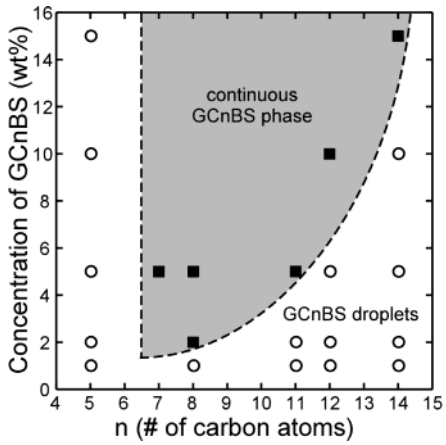

Figure 7. PS/GC*n*BS blend microstructures plotted as a function of concentration (wt %) and the number of carbon atoms in the GC*n*BS alkyl chain. Open circles denote blends consisting of droplets of GC*n*BS in a PS matrix; filled squares denote microstructures that are continuous in GC*n*BS. The dotted line outlines the region of phase space in which GC*n*BS continuous phases occur. Although the ordinate here has units of wt %, the inscribed continuous phase region is not an artifact of the different molar masses of the smectic components.

Table 2. Length (*L*), Diameter (*D*), and Droplet Aspect Ratio (*L*/*D*) of Extended Droplets in PS/GC*n*BS Blends

	L (μm)[a]	*D* (μm)[b]	*L*/*D*
PS/5% GC5BS	3.6	1.02	3.5
PS/5% GC12BS	8.0	0.53	15.1
PS/5% GC14BS	4.7	0.52	9.0

[a] The standard deviations associated with *L* for PS/5% GC5BS, PS/5% GC12BS, and PS/5% GC14BS were 3.2, 6.6, and 3.0, respectively. [b] The standard deviations associated with *D* for PS/5% GC5BS, PS/5% GC12BS, and PS/5% GC14BS were 0.69, 0.36, and 0.36, respectively.

accompanied by pronounced delamination of the outer surfaces of the plaque. This delamination was evident when viewed along either the perpendicular or parallel direction (with respect to injection). The formation of large, thin sheets of GC*n*BS material during injection molding is due to the effect of large extensional stresses present at the advancing front of the molten blend. As the GC*n*BS droplets approach the front, they experience significant extensional stresses and are swept from the center of the flow to the wall region, a phenomena known as fountain flow (Figure 11).[35,36] The role of the extreme extensional stresses was confirmed by the absence of large-scale lamella in samples prepared in a 2 mm thick mold, in which the stresses would be significantly reduced. Large sheets of PS with thicknesses of approximately 100 μm and areas equal to the plaque area can be peeled easily from the surface of the plaque, revealing stratification of the polymer due to the formation of continuous lamellae of the smectic phase during molding (Figure 12). Concentration of the smectic phase in the blend and the length of the GC*n*BS alkyl chains also appear to play important roles in the polymer stratification. Delamination is observed for PS/2% GC11BS and PS/5% GC14BS blends, but not for PS/2% GC14BS. All the smectic-containing blends, however, form GC*n*BS platelets. It is important to note that blends in the "continuous GC*n*BS phase" regime (Figure 7) could not be successfully injection molded.

Conclusions

The production of polymer composite materials with predictable physical properties depends on the ability to control the composite microstructure in a reproducible manner. The results described herein demonstrate that properly designed smectic phases, when blended with polystyrene, produce significant changes in the blend rheology with respect to the pure polymer. The effect of the smectic component on the rheological properties is especially pronounced at GC*n*BS concentrations that promote the formation of a microstructure characterized by a GC*n*BS continuous phase and a discontinuous polymer phase. The formation of this GC*n*BS continuous phase is accompanied by a large interfacial contact area between the polymer and smectic phases. The dependence of blend microstructure on alkyl chain length appears to indicate differences in the PS−GC*n*BS

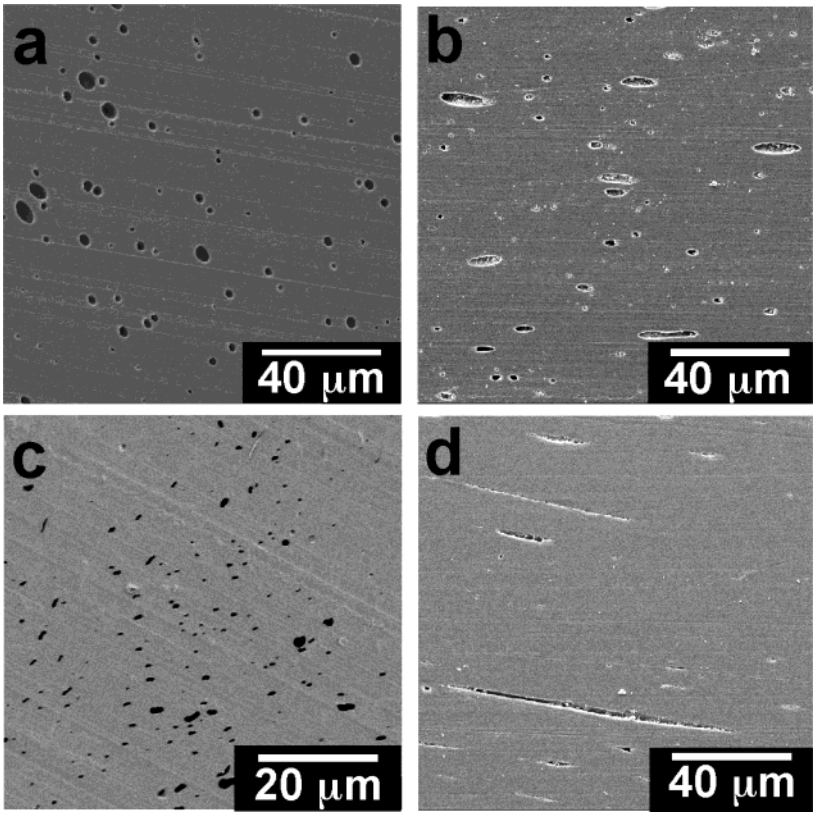

Figure 8. SEM images of extruded blends after the removal of GC*n*BS by dissolution in methanol: (a) PS/5% GC5BS sample cut perpendicular to the direction of flow and (b) sample cut parallel to the direction of flow; (c) PS/5% GC12BS sample cut perpendicular to the direction of flow and (d) sample cut parallel to the direction of flow.

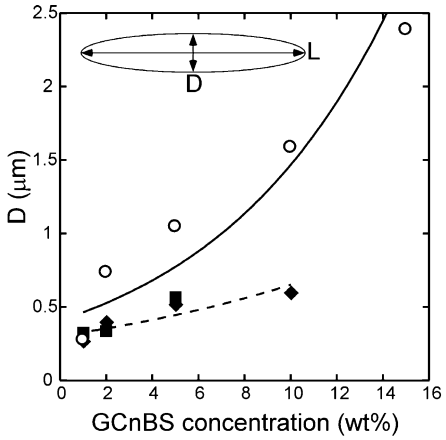

Figure 9. Droplet diameter *D* (as measured from SEM images) of blends of PS with GC5BS (○), GC12BS (■), and GC14BS (◆).

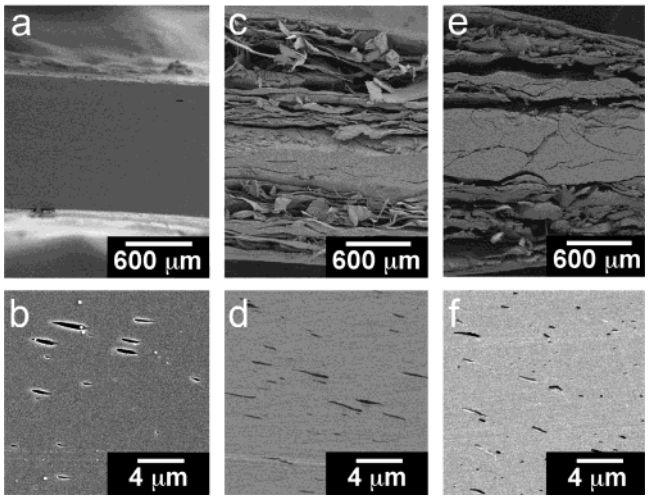

Figure 10. SEM images of injection-molded samples after removal of GC*n*BS from the blend with methanol. (a, b) The PS/2% GC5BS plaque, imaged in direction perpendicular to flow, and a higher magnification view of the plaque center. (c, d) The PS/2% GC11BS plaque imaged in direction perpendicular to flow and a higher magnification view of the plaque center. (e, f) A PS/2% GC11BS plaque imaged in direction parallel to flow and a higher magnification view of the plaque center from the same orientation. In the smectic-containing blends, the outer surfaces exhibit delamination, but the inner surfaces exhibit features that signify the existence of dispersed smectic platelets. In contrast, the blend containing GC5BS, which does not form a smectic phase, exhibits platelets in the interior but does not exhibit delamination.

interfacial tension. Although the results described herein were limited to polystyrene, parallel experiments have revealed the formation of similar GC*n*BS continuous phases in both polypropylene and high-density polyethylene. The layered structure inherent in the GC*n*BS smectic and crystalline phases can be exploited to form rather extensive lamellar microstructures during injection molding. The tendency to form these microstructures depends on both alkyl chain length and concentration, the former probably reflecting different polymer−smectic interfacial energies for different values of *n*. Upon cooling, these lamellar microstructures afforded stratified polymer plaques due to formation of extended two-dimensional domains of GC*n*BS crystals. These observations suggest that blends based on smectic phases that can be designed at the molecular level may find use in applications that rely on reduced gas permeability. The delamination observed in the stratified polymer plaques places some limitation on the applicability of these composite systems; however, we

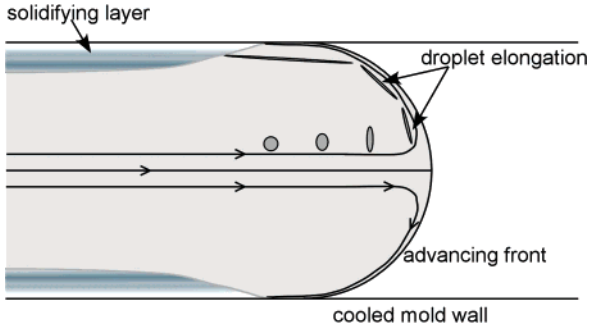

Figure 11. Schematic of the fountain flow phenomena observed in injection molding of polymer melts. Droplets located in the center of the mold are elongated by extensional stresses experienced as they reach the advancing front and are eventually swept to the wall region of the mold where they solidify as large lamellae.

Figure 12. A sheet of polystyrene peeled from the outer surface of an injection molded PS/2% GC11BS plaque.

anticipate that by varying the length and chemistry of the organosulfonate and the nature of the polymer matrix, the adhesion between the two phases may be improved.

Experimental Section

Composite Preparation. Guanidinium alkylbenzenesulfonates (GC*n*BS) were synthesized by sulfonation of commercially obtained alkylbenzenes (Sigma-Aldrich, Milwaukee, WI) using procedures previously reported for other substituted benzenesulfonates and benzenedisulfonates.[37,38] Polystyrene (Dow Chemical, Styron 685: MFR 2.5), high-density polyethylene (Dow Chemical, 12450), polypropylene (Huntsman, H0500, MFR 5), and an antioxidant (Ciba Specialty Chemicals, Irganox 1010) were used as received. Polystyrene/GC*n*BS composites were prepared by blending polystyrene (PS), GC*n*BS, and Irganox1010 (<0.1 wt %) in a twin-screw microcompounder (DACA) for 10 min at a temperature of 220 °C and a mixing speed of 50 rpm (a shear rate of ~10 s^{-1}) under a nitrogen atmosphere. The resulting blends were extruded through a cylindrical die to generate ~2 mm diameter strands. These strands then were placed in the cylindrical reservoir of a microinjector (DACA) and heated to 220 °C. After 10 min the molten mixture was injected at a pressure of 500 kPa into a rectangular mold at 70 °C, thereby quickly quenching the melt. Two rectangular molds of different thickness (20 mm × 75 mm × 1 mm and 20 mm × 75 mm × 2 mm) were used to compare the effect of shear stress on the composite microstructure and properties. The same procedure was used to prepare composites based on polyethylene and polypropylene as well as pure polymer samples, which were used for comparison purposes.

Materials Characterization. The polymer glass transition temperatures (T_m) and the isotropic melting and smectic transition temperatures ($T_{C\rightarrow I}$ and $T_{C\rightarrow S}$, respectively) of the GC*n*BS compounds were determined by differential scanning calorimetry (Perkin-Elmer DSC7) using a scan rate of 10 °C/min. The existence of crystalline GC*n*BS compounds in the blends was verified by wide-angle powder X-ray diffraction (PXRD, Bruker-AXS D5005 powder X-ray diffractometer). These measurements also confirmed that the crystal structures of the GC*n*BS compounds in the blends were identical to those of their corresponding pure bulk materials. The GC*n*BS smectic phases in the blends were characterized at the processing temperatures by powder X-ray diffraction (Scintag XDS 2000 X-ray diffractometer equipped with a temperature-controlled sample stage and a theta−theta goniometer). The rheological properties of the polymer/GC*n*BS blends were measured at 220 °C using a rheometer (Rheometric Scientific ARES II) setup with a parallel plate geometry (25 mm diameter, 0.7 mm gap). Transient shear step rate tests were performed at 220 °C and at shear rates between 0.01 and 1 s^{-1}.

The microstructures of the polymer/GC*n*BS blends were characterized by scanning electron microscopy (SEM, JEOL 6500). The samples were prepared by microtoming the composites (Reichert Ultramicrotome equipped with a glass knife), followed by immersion in methanol for 24 h to dissolve the GC*n*BS component and develop domains that were replicas of the GC*n*BS component. The samples were coated with platinum (ca. 5 nm thickness) prior to imaging. The SEM images were analyzed with UTHSCSA Image Tool (Version 3, The University of Texas Health Science Center at San Antonio). Specifically, the cross-sectional area (A), lengths (L), diameter (D), and equivalent sphere diameters (R_0) of the empty domains, which previously had contained the GC*n*BS component, were measured automatically by image analysis of each blend; 200−600 particles were analyzed in order to obtain statistically meaningful values. The cross-sectional diameter was calculated using eq 2.

$$L_2 = 2\sqrt{A/\pi} \tag{2}$$

Acknowledgment. This work was supported by the National Science Foundation (DMR-0305278) and the Sundahl Fellowship (S.M.M.) and Asahi Kasei Corp. (J.Y.). We thank Frédéric Lortie for helpful discussions, Thuy Chastek for her technical advice with SEM, and David Giles for help with the rheology measurements.

References and Notes

(1) Dutta, D.; Fruitwala, A.; Kohli, A.; Weiss, R. A. *Polym. Eng. Sci.* **1990**, *30*, 1005.
(2) Coles, M. J.; Carboni, C.; Coles, H. J. *Liq. Cryst.* **1999**, *26*, 679.
(3) Leader, C. M.; Zheng, W.; Tipping, J.; Coles, H. J. *Liq. Cryst.* **1995**, *19*, 415.
(4) Drzaic, P. *J. Appl. Phys.* **1986**, *60*, 2142.
(5) Molsen, H.; Kitzerow, H.-S. *J. Appl. Phys.* **1994**, *75*, 710.
(6) Stannarius, R.; Crawford, G. P.; Chien, L. C.; Doane, J. W. *J. Appl. Phys.* **1991**, *70*, 135.
(7) Mucha, M. *Prog. Polym. Sci.* **2003**, *28*, 837.
(8) Berry, G. C. *Trends Polym. Sci.* **1996**, *4*, 289.
(9) Roetting, O.; Hinrichsen, G. *Adv. Polym. Technol.* **1994**, *4*, 279.
(10) Pawlikowski, G. T.; Dutta, D.; Weiss, R. A. *Annu. Rev. Mater. Sci.* **1991**, *21*, 159.
(11) Frederickson, G. H.; Bicerano, J. *J. Chem. Phys.* **1999**, *110*, 2181.
(12) Fornes, T. D.; Paul, D. R. *Polymer* **2003**, *44*, 4993.
(13) Lortie, R.; Macosko, C. W. *Polym. Eng. Sci.*, submitted for publication.
(14) Brunsveld, L.; Folmer, B. J. B.; Meijer, E. W.; Sijbesma, R. P. *Chem. Rev.* **2001**, *101*, 4071.
(15) Thierry, A.; Straupe, C.; Lotz, B.; Wittman, J. C. *Polym. Commun.* **1990**, *31*, 299.
(16) Shepard, T. A.; Delsorbo, C. R.; Louth, R. M.; Walborn, J. L.: Norman, D. A.; Harvey, N. G.; Spontak, R. J. *J. Polym. Sci., Part B: Polym. Phys.* **1997**, *35*, 2617.
(17) Bauer, T.; Thomann, R.; Mülhaupt, R. *Macromolecules* **1998**, *31*, 7651.

(18) Fuchs, K.; Bauer, T.; Thomann, R.; Wang, C.; Fredrich, C.; Mulhaupt, R. *Macromolecules* **1999**, *32*, 8404.
(19) Subramanaina, P. M.; Plotzker, I. G. In *Polymer Blends*; Paul, D. R., Bucknall, C. B., Eds.; Wiley-Interscience: New York, 2000; Vol. 2, p 359.
(20) Flodberg, G.; Hedenqvist, M. S.; Gedde, U. W. *Polym. Eng. Sci.* **2003**, *43*, 1044.
(21) Russell, V. A.; Etter, M. C.; Ward, M. D. *J. Am. Chem. Soc.* **1994**, *116*, 1941.
(22) Swift, J. A.; Pivovar, A. M.; Reynolds, A. M.; Ward, M. D. *J. Am. Chem. Soc.* **1998**, *24*, 5887.
(23) Evans, C. C.; Sukarto, L.; Ward, M. D. *J. Am. Chem. Soc.* **1999**, *121*, 320.
(24) Holman, K. T.; Pivovar, A. M.; Ward, M. D. *Science* **2001**, *294*, 1907.
(25) Mathevet, F.; Masson, P.; Nicoud, J. F.; Skoulios, A. *Chem.—Eur. J.* **2002**, *8*, 2248.
(26) Russell, V. A.; Etter, M. C.; Ward, M. D. *Chem. Mater.* **1994**, *6*, 1206.
(27) Martin, S. M.; Horner, M. J.; Yonezawa, J.; Macosko, C. W.; Ward, M. D. *Chem. Mater.*, in press.
(28) Jahromi, S.; Moosheimer, U. *Macromolecules* **2000**, *33*, 7582.
(29) Jadzyn, J.; Dabrowski, R.; Lech, T.; Czechowski, G. *J. Chem. Eng. Data* **2001**, *46*, 110.
(30) Chapoy, L. L.; Duke, R. W. *Rheol. Acta.* **1979**, *18*, 537.
(31) Koning, C.; Van Duin, M.; Pagnoulle, C.; Jerome, R. *Prog. Polym. Sci.* **1998**, *23*, 707.
(32) Using a simple geometrical model in which spherical polymer domains of diameter D are surrounded by a smectic "shell", the thickness, d, of the shell is defined by the following equation: $d = (D/2)[(1 + x/(1 - x))^{1/3} - 1]$, where x is the volume fraction of the smectic phase. The choice of a domain diameter $D = 200\ \mu$m is a conservative one, as many of the domains are in fact larger in size. Larger domain sizes would result in an even larger estimate of the shell thickness d.
(33) Taylor, G. I. *Proc. R. Soc. London* **1934**,*146*, 501.
(34) The capillary number is defined as $Ca = \eta_m \dot{\gamma} R_0/2\sigma$, where η_m is viscosity of the polymer matrix, $\dot{\gamma}$ is the applied shear rate, σ is the interfacial tension, and R_0 is the equivalent sphere diameter of extended droplets calculated using the following relation: $R_0 = ({}^3/_2 LD^2)^{1/3}$. See: Taylor, G. I. *Proc. R. Soc. London* **1934**, *146*, 501.
(35) Tadmor, Z.; Gogos, C. G. *Principles of Polymer Processing*; John Wiley and Sons: New York, 1979.
(36) Wilkinson, A. N.; Ryan, A. J. *Polymer Processing and Structure Development*; Kluwer Academic Publishers: Boston, 1998.
(37) Holman, K. T.; Martin, S. M.; Parker, D. P.; Ward, M. D. *J. Am. Chem. Soc.* **2001**, *123*, 4421.
(38) Plaut, D. J.; Martin, S. M.; Kjaer, K.; Weygand, M. J.; Lahav, M.; Leiserowitz, L.; Weissbuch, I.; Ward, M. D. *J. Am. Chem. Soc.* **2003**, *125*, 15922.

MA0493729